

PAPER

Frequency analysis of hexagonal microbeam with 2D nanofiber mat

To cite this article: Aparna Gangele *et al* 2019 *Mater. Res. Express* **6** 085631

View the [article online](#) for updates and enhancements.



IOP | ebooks™

Bringing you innovative digital publishing with leading voices to create your essential collection of books in STEM research.

Start exploring the collection - download the first chapter of every title for free.

Materials Research Express



PAPER

Frequency analysis of hexagonal microbeam with 2D nanofiber mat

RECEIVED
4 February 2019

REVISED
25 May 2019

ACCEPTED FOR PUBLICATION
7 June 2019

PUBLISHED
19 June 2019

Aparna Gangele^{1,4}, Akarapu Ashok^{1,4} , Chandra Sekhar Sharma² , Prem Pal³ and Ashok Kumar Pandey¹

¹ Department of Mechanical and Aerospace Engineering, IIT Hyderabad, Kandi, Sangareddy 502285, India

² Department of Chemical Engineering, IIT Hyderabad, Kandi, Sangareddy 502285, India

³ Department of Physics, IIT Hyderabad, Kandi, Sangareddy 502285, India

⁴ These authors have equal contributions.

E-mail: ashok@iith.ac.in

Keywords: 2D nanofiber mat, MEMS, vibration

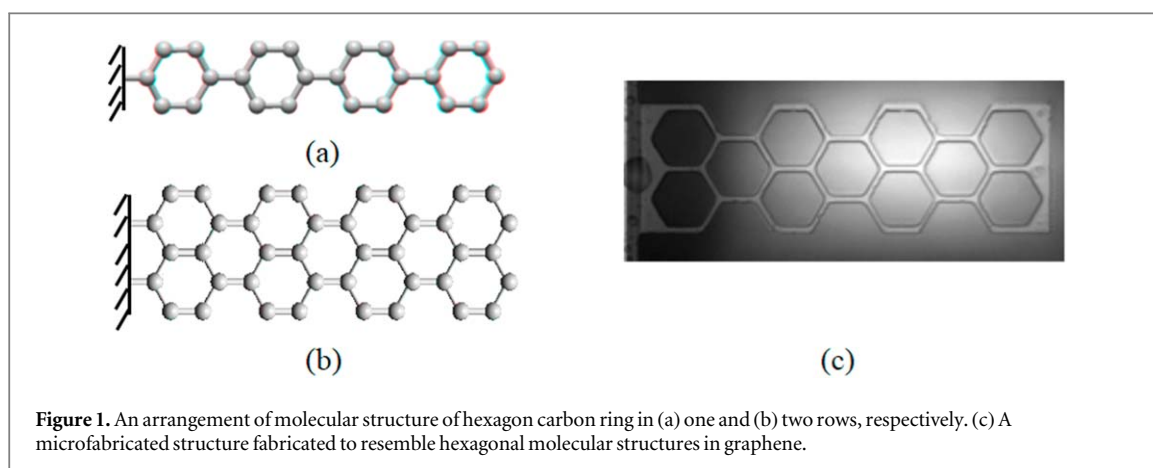
Abstract

Flexibility of graphene (Gr) is partially credited to its two-dimensional (2D) molecular structure which resembles like interconnected unit of hexagonal carbon atoms ring. Therefore, to increase the flexibility of micromechanical beams, we analyze the influence of hexagonal shape of microcantilever beam without and with hexagonal hole of varying side length. To carry out the analysis, we first fabricate the hexagonal structure and perform measurement using laser vibrometer. Based on the measurement, we found that the presence of hexagonal holes make the beam flexible by two order of magnitude more than that of a conventional beam without holes. However, we found that the frequency of microcantilever beam with hexagonal shape decreases with increase in hole size. To undo the effect of hexagonal holes on microbeam frequency, we cover the microbeam with an electrospun cellulose acetate nanofiber mat (CAF). Based on the measurements, we found that the frequency can be increased more than that of a solid rectangular microbeam. Finally, we propose a finite element based methodology to model microbeam and nanofiber mat to compute their frequencies. Thus, based on the understanding developed in this work, this hierarchical structure of microcantilever beam with electrospun nanofibers can be used as a best candidate for utilizing it for the development of flexible sensors based on MEMS devices.

1. Introduction

With improvement in micro and nanofabrication processes, researchers can control the growth of single or arrays of nanotubes or nanofibres effectively [1–3]. With such advancement, there had been significant research in finding out various properties of such nanofibers and nanotubes in order to use them for different applications like energy, light weight composites, nanoelectronics, biotechnology, etc [4]. Some used it as single-walled carbon nanotube (SWCNT) and double-walled carbon nanotube (DWCNT) for designing resonators [5], others used them in the form of arrays such as vertically aligned carbon nanotubes (VACNTs) to increase the surface areas [6–9]. Subsequently, many researchers have started using excellent properties of carbon in order to improve the mechanical properties of other planer structures such as microelectromechanical system (MEMS) or nanoelectromechanical system (NEMS) which are much easier to control as compared to nanofibers and nanotubes [10–13]. Now, there has been series of ideas for graphene-based and horizontally aligned nano and micro devices in the field of flexible sensors and actuators. To design efficient flexible resonant sensors, different mechanisms of controlling resonance frequency as well as flexibility should be explored. In this paper, we explore the effect of hexagonal shape on the flexibility of beam and discuss the influence of nanofiber mat on the frequency.

Many researchers credit hexagonal shape of graphene to its mechanical excellent properties. A layer of graphene resembles like interconnected unit of hexagonal carbon atoms ring as shown in figures 1(a) and (b). Therefore, we aim to explore the performance of hexagonal microcantilever beam fabricated using microfabrication processes on its flexibility and vibrational characteristics. With the progress of flexible devices,



the demand for integrating MEMS devices with flexible substrate has been on the rise. With unique mechanical and electrical properties of graphene (Gr) and carbon nanotube (CNT) [14], there have been efforts to achieve large Gr and aligned CNT array based silicon and other polymer substrate like PMMA through certain techniques [15] so as to integrate it with other MEMS based devices [16, 17]. While there have been some success in achieving the above goals with Gr and CNTs array [18, 19], other nanomaterial such as cellulose acetate (CA) based nanofiber [20] may come handy in achieving this goal with some better controllability for achieving large flexible devices. However, its integration with micro or nanodevices need to be investigated. In this work, we discuss about the effect of integrating CA based nanofiber on hexagonal shape microbeams.

To analyze the integration of nanofiber mats with microdevices, we first fabricate rectangular microcantilever beams with and without hexagonal holes using microfabrication techniques. After that we transfer the nanofiber mats with different concentration/density on microcantilever beam. Subsequently, we perform experiments to measure the frequencies and quality factor with and without nanofibers. To perform numerical analysis, we model the microbeam and nanofiber using finite element method in ANSYS. The interface is modelled using bonded contact model. After extracting the mechanical properties of nanofibers based on the comparison of numerical and experimental results, we analyze the influence of thickness and boundary conditions of nanofiber on the frequencies of combined microbeam and nanofiber mat.

2. Methodology

In this section, we describe the fabrication and measurement procedure of silicon dioxide microbeam with and without nanofiber mats. Subsequently, we describe numerical procedure to model nanofiber mat, silicon dioxide beam, and its interface.

2.1. Fabrication and measurement procedure

For the fabrication of silicon dioxide microbeam, Czochralski (Cz) grown 4-inch diameter P-type boron doped (resistivity 8–12 Ωcm) {100} oriented single side polished silicon wafers were used. In the micromachining process, in order to utilize silicon dioxide (SiO_2) as structural and masking material, SiO_2 of about 1 μm thickness was grown using thermal oxidation process. The step by step fabrication process for the fabrication of silicon dioxide (SiO_2) hanging structures is described in figure 2(a) [21]. Using UV photolithography (Midas Mask Aligner, MDA 400 M) technique, the geometric patterns were transferred onto the oxidized wafer coated with positive photoresist. This step is followed by silicon dioxide etching in buffered hydrofluoric acid (BHF) solution. Later the patterned full wafer was diced into small chip size samples of size $2 \times 2 \text{ cm}^2$. As diced chip sized samples are cleaned in piranha ($\text{H}_2\text{SO}_4\text{:H}_2\text{O}_2\text{:1:1}$) solution followed by rinsing with deionized (DI) water. The chemical oxide of few nanometer thickness which generates on silicon surface due to the piranha cleaning is removed by immersing the sample in 1% hydrofluoric acid (HF) solution which is followed by thorough rinse of the sample in DI water. Finally etching is performed in 25 wt% TMAH (Tetramethylammonium hydroxide) (99.999%, Alfa Aesar) at $74.5 \pm 0.5 \text{ }^\circ\text{C}$ to fabricate overhanging SiO_2 microcantilevers. After etching process the samples were rinsed with DI water. Figure 2(b) shows an image of a honeycomb beam with hexagonal holes fabricated using microfabrication processes as explained above. The thickness of microbeam is measured using ellipsometer (JA Woolam, model: M-2000D). In this study, we fabricated beams with thicknesses 0.97 μm and 0.962 μm . It is due to differences in etching time of two different chips/die. Subsequently, we use laser scanning vibrometer (Polytec, OFV-5000 vibrometer) setup as described in figure 2(c) to measure the frequency response curve as shown in figure 2(d) when the structure is subjected to pseudorandom excitation provided by

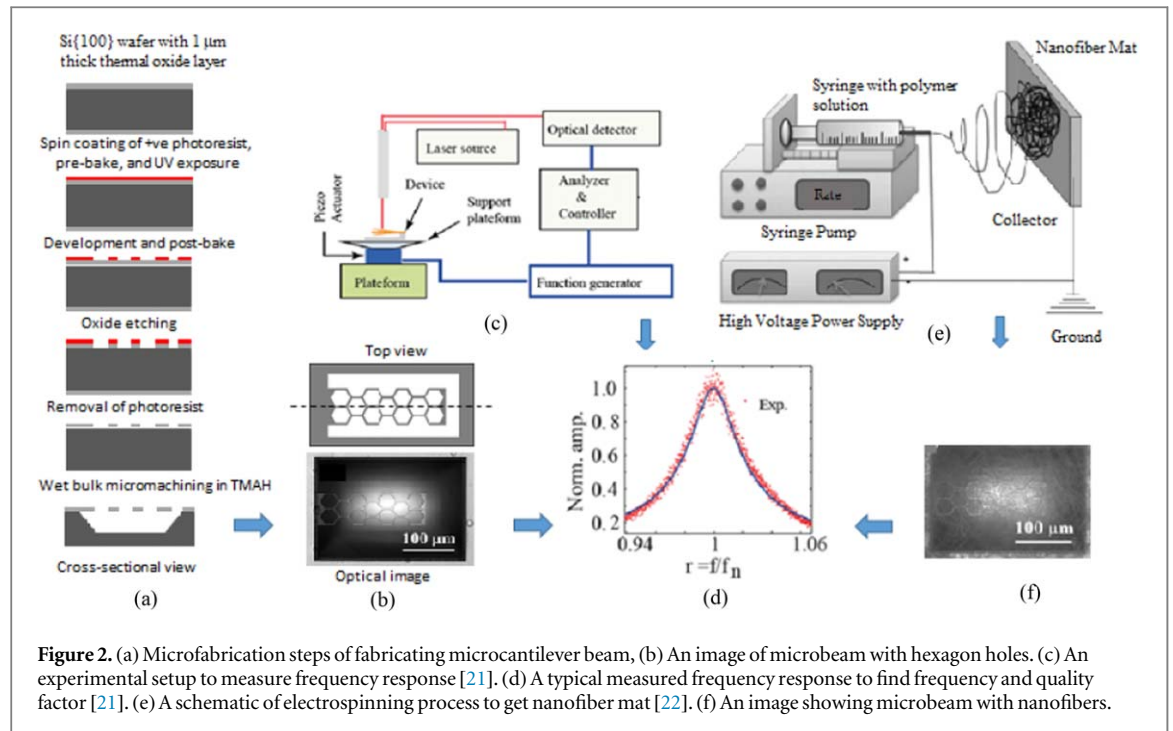


Figure 2. (a) Microfabrication steps of fabricating microcantilever beam, (b) An image of microbeam with hexagon holes. (c) An experimental setup to measure frequency response [21]. (d) A typical measured frequency response to find frequency and quality factor [21]. (e) A schematic of electrospinning process to get nanofiber mat [22]. (f) An image showing microbeam with nanofibers.

piezoelectric patches through the platform over which the test device is kept [21]. The measurement is performed under vacuum condition with pressure of 9×10^{-3} mbar. From the measured frequency response, we measure modal resonance frequency and quality factor of the test structure corresponding to a given mode shape of the microcantilever beam.

To fabricate nanofiber mats, we use electrospinning technique which is a simple and cheap method to fabricate fibers with varying diameter from micro to nanoscale [23] under the influence of a high voltage as shown in figure 2(e). Using this method, a polymer fiber with charged droplet from solution is ejected and collected on a copper substrate kept on a grounded collector to form sheet like nanofiber mats. The shape, size and density of nanofiber mats using electrospinning process can be varied by controlling different parameters such as concentration, additives, flow-rate, humidity, viscosity, surface tension, applied voltage, and gap between nozzle to grounded collector [22–25]. After electrospinning the nanofibers on the copper substrate, the fibers were transferred onto the silicon chip containing different designs of SiO₂ microcantilever beams by using a stainless steel tweezer. Figure 2(f) shows an image of microcantilever beam with nanofiber mats. Subsequently, we measure the frequency and quality factor of microbeam with nanofiber mat from its measured frequency response.

2.2. Numerical procedure

In this section, we develop finite element models in ANSYS [26] for analyzing the vibrational characteristics of different microbeam structures with and without nanofiber mat. From modeling perspective of a silicon dioxide beam with nanofiber, it can be considered into three different layers, namely, a bottom silicon dioxide beam, a top nanofiber mat and an interfacial layer between beam and fiber mat as shown in figure 3(a). Subsequently, a correct boundary condition (B.C.) similar to the original condition has to be found. A typical bottom view can be shown in figure 3(b).

2.2.1. Silicon dioxide beam

To model silicon dioxide beams, the material properties used in the present work are 66.26 GPa for elastic modulus, 30.12 GPa for shear modulus, 2200 kg m^{-3} for density and 0.1 for Poisson's ratio which are found based on the comparison of analytical and experimental values of frequencies [27]. Shell 181 element, a four-node element with six degrees of freedom per node, is used to model silicon dioxide beam. A quadratic type mesh element is utilized in the meshing process. Modal analysis is done to compute modal frequencies. The mesh convergence is achieved for around 2000 number of elements with percentage error of less than 1% when compared with converged results.

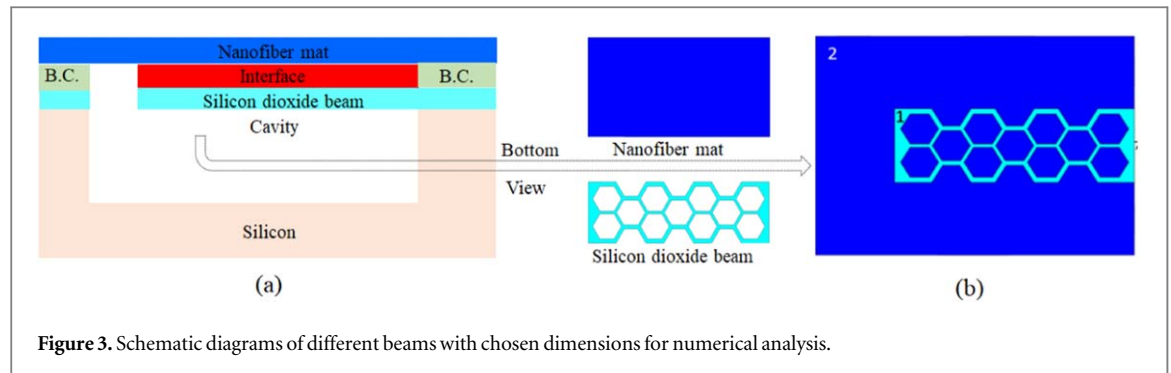


Figure 3. Schematic diagrams of different beams with chosen dimensions for numerical analysis.

2.2.2. Cellulose acetate nanofiber mat

To model electrospun cellulose acetate nanofibers (CAFs) in the form of thin layer of mat, we use shell 181 element same as that used in modeling silicon dioxide beam. The bulk properties of CAF are captured by modeling it as continuum without considering any specific arrangement of fibers, their diameter, and porosity of mats to reduce the complexity and computational effort. Based on the comparison of experimental and measured values of frequencies, we found the material properties such as elastic modulus as 120 MPa, density as 1.28 g cm^{-3} and Poisson's ratio as 0.3 which are found to be in the acceptable range of measured properties of CAFs found in the literature [28, 29]. One can further consider other related effects such as the influence of fiber arrangement, nanofiber diameter, nanofiber mat porosity, etc., which are beyond the scope of present study.

2.2.3. Interface and boundary condition

To model interface region between the top surface of silicon dioxide beam and bottom surface of CAFs mat, we use bonded contact element with suitable contact pair. The detail about using this element has been discussed in detail in previous chapters for modeling interfaces of different nanocomposites [30] in which the two contacting surfaces are assumed to be bonded together throughout the analysis. It uses augmented Lagrange contact algorithm for the contact elements. In this study, the contact modelling is performed using the ANSYS contact pair by choosing the 3D TARGE170 and node-to-surface CONTA175 elements to model the interface. The nodes of the cellulose acetate nanofiber mesh are assumed as contact nodes and are modelled with CONTA175 element, and the surface of the silicon dioxide beam is assumed as a target surface and is modelled with TARGE170 element. Furthermore, as the fiber mat is simply transferred physically with tweezer from copper substrate to silicon dioxide, the simply-supported boundary condition can be assumed. However, we analyze the influence of free-free boundary condition, simply-supported boundary condition with and without zero slope to validate the selection of appropriate boundary condition.

3. Results and discussion

In this section, we first analyze the influence of hexagonal shaped microbeam on its fundamental bending mode without holes using numerical and analytical modeling. Subsequently, we study the influence of hole size in hexagonal shaped honeycomb microcantilever beam based on numerical simulation. Subsequently, we compare numerical results with experimental results for beams with and without holes. Further, after performing static analysis to find deflection corresponding to a given concentrated load, we carry out detail numerical analysis of microbeams with and without nanofiber mat of different concentration. Finally, the results are compared with experiments and further analysis is presented.

3.1. Frequency analysis of hexagonal microcantilever beams

To systematically perform the influence of hexagonal shape on the frequency of microcantilever beam, we take hexagonal beam of different lengths as shown in figure 4(a). Beams termed as S-I, S-II, S-III, S-IV, and S-V have net lengths of $45 \mu\text{m}$, $105.63 \mu\text{m}$, $166.26 \mu\text{m}$, $226.89 \mu\text{m}$. While the width of beams represented by S-I, S-II, S-III and S-IV is $38.97 \mu\text{m}$, the width of beam denoted by S-V is $77.94 \mu\text{m}$. Each hexagon has a side length of $22.5 \mu\text{m}$ and any two adjacent hexagons are interconnected by a uniform beam of length $17.35 \mu\text{m}$ and width $2.975 \mu\text{m}$. Based on the modal analysis performed using ANSYS, we compute modeshape of the beams corresponding to first bending mode as shown in figure 4(b). The frequencies of all the beams as shown in figure 4(a) and their equivalent rectangular counterparts are tabulated in table 1. A comparison of results shows that frequency of beam S-I is more than that of rectangular counterpart but frequencies of other beams reduce. Thus, hexagonal beams with more than one hexagonal component become more flexible as compared to their

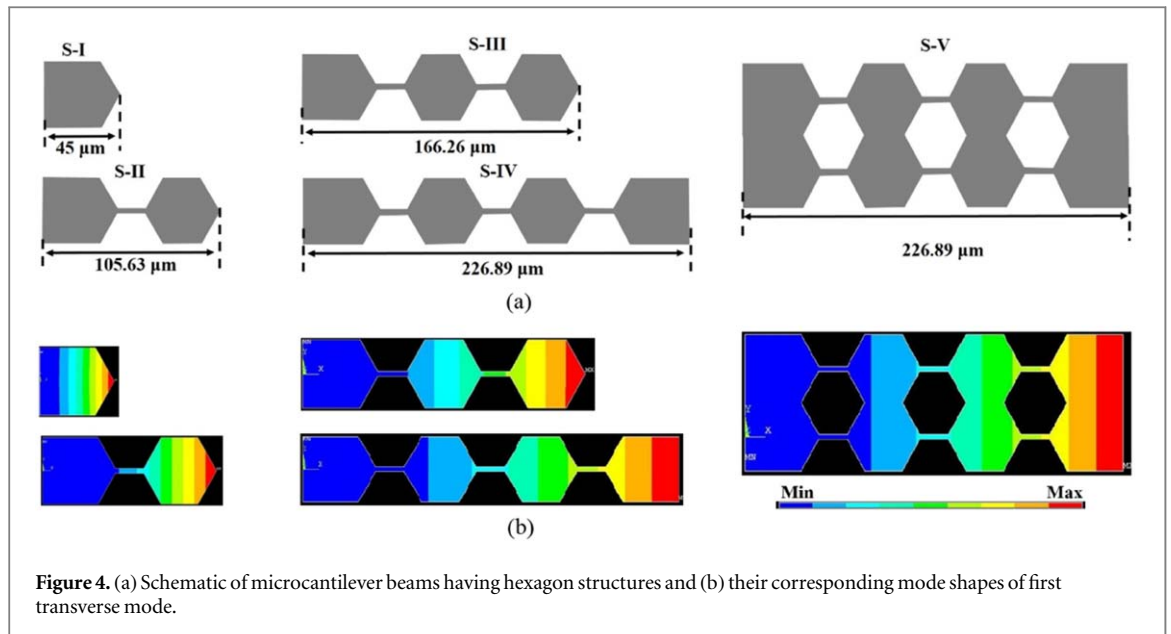


Figure 4. (a) Schematic of microcantilever beams having hexagon structures and (b) their corresponding mode shapes of first transverse mode.

Table 1. Comparison of numerical and analytical resonance frequencies corresponding to first transverse mode for the beams shown in figure 4, also comparing with frequency of their equivalent rectangular shaped beams.

Details of the cantilever beam	Resonance frequency (kHz)	
	Numerical/analytical	Equivalent rectangular beam, numerical
S ₁	541.10/565.23	422.49
S ₂	59.74/57.57	76.60
S ₃	20.80/17.10	30.90
S ₄	9.79/8.14	16.58
S ₅	9.79/—	16.60

rectangular counterparts. To approximately compute the analytical results of beams shown in figure 4(a), we take $k_{\text{eff}} = \frac{E \times wt^3}{4L^3}$ and $m_{\text{eff}} = 0.23m_{\text{total}}$, respectively, to compute frequency from $f = \frac{1}{2\pi} \sqrt{\frac{k_{\text{eff}}}{m_{\text{eff}}}}$ and are compared with numerical results in table 1. The approximate analytical models give percentage error of 4.4%, 3.6%, 17.7%, and 16.85%, respectively, for beams S-I, S-II, S-III and S-IV. Based on the comparison, we also found that any increase in width, as in the case of beam S-V, has negligible effect on its frequency.

3.2. Static and frequency analysis of microbeam with holes

To study the influence of hexagonal hole of side length 'a' on static deflection and frequency, we fabricate honeycomb-shaped hexagonal beam of type S-V (shown in figure 4(a)) without any hole and with holes of side length $a = 16.55 \mu\text{m}$ as shown in figures 5(a) and (b). The overall length of the beam is $175.525 \mu\text{m}$ and its width and thickness are $76.72 \mu\text{m}$ and $0.962 \mu\text{m}$, respectively.

To understand the influence of different hole shapes, we numerically perform the static analysis of hexagonal beam with and without hexagonal holes, circular holes, square holes, and its equivalent rectangular beam. To perform the static analysis of these beams in ANSYS, a constant load of $100 \mu\text{N}$ is applied at the free end of cantilever beam while the other end is fixed. Figure 5(c) illustrates the comparison of deflection obtained for the honeycomb-shaped microcantilever beams, equivalent rectangular beam and beams with different hole shapes. From the graph, it can be observed that for the given load the deflection produced in honeycomb shaped cantilever beam without holes as shown in figure 5(a) is only 35% higher than that produced in equivalent rectangular beam. However, the deflection produced in honeycomb shaped cantilever beam having the hexagon hole with side length of $a = 16.55 \mu\text{m}$ as shown in figure 5(b) is about 454.18% higher than that produced by its equivalent rectangular cantilever beam. Furthermore, figure 5(c) also shows the comparison of beam with hexagonal, square and circular shaped holes for the two cases. In the first case, side length or diameter of the

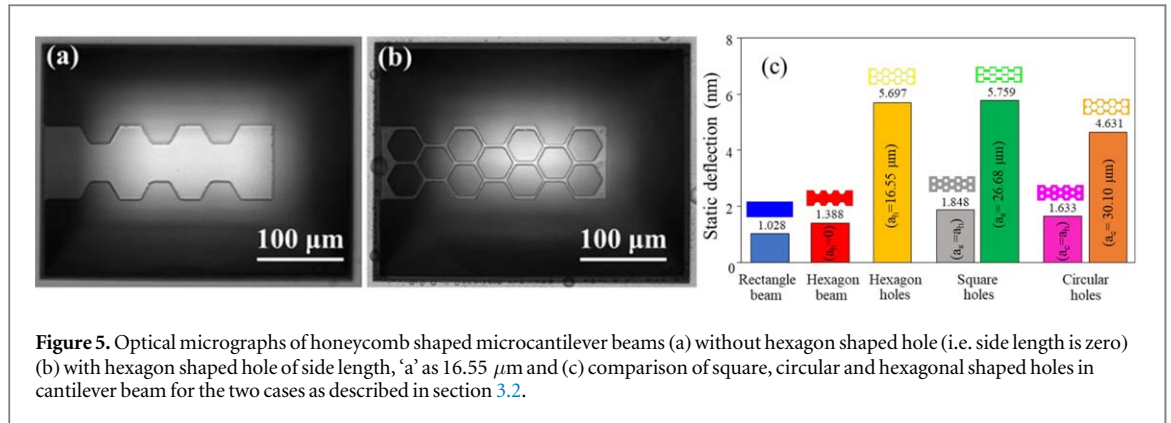


Figure 5. Optical micrographs of honeycomb shaped microcantilever beams (a) without hexagon shaped hole (i.e. side length is zero) (b) with hexagon shaped hole of side length, 'a' as 16.55 μm and (c) comparison of square, circular and hexagonal shaped holes in cantilever beam for the two cases as described in section 3.2.

Table 2. Comparison of experimental and numerical resonance frequencies corresponding to first transverse and torsional modes for honeycomb shaped microcantilever beams having different hexagon side lengths.

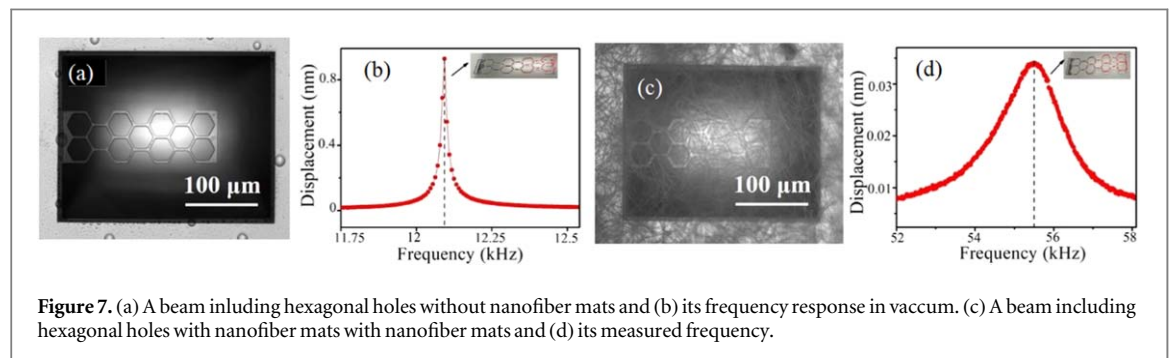
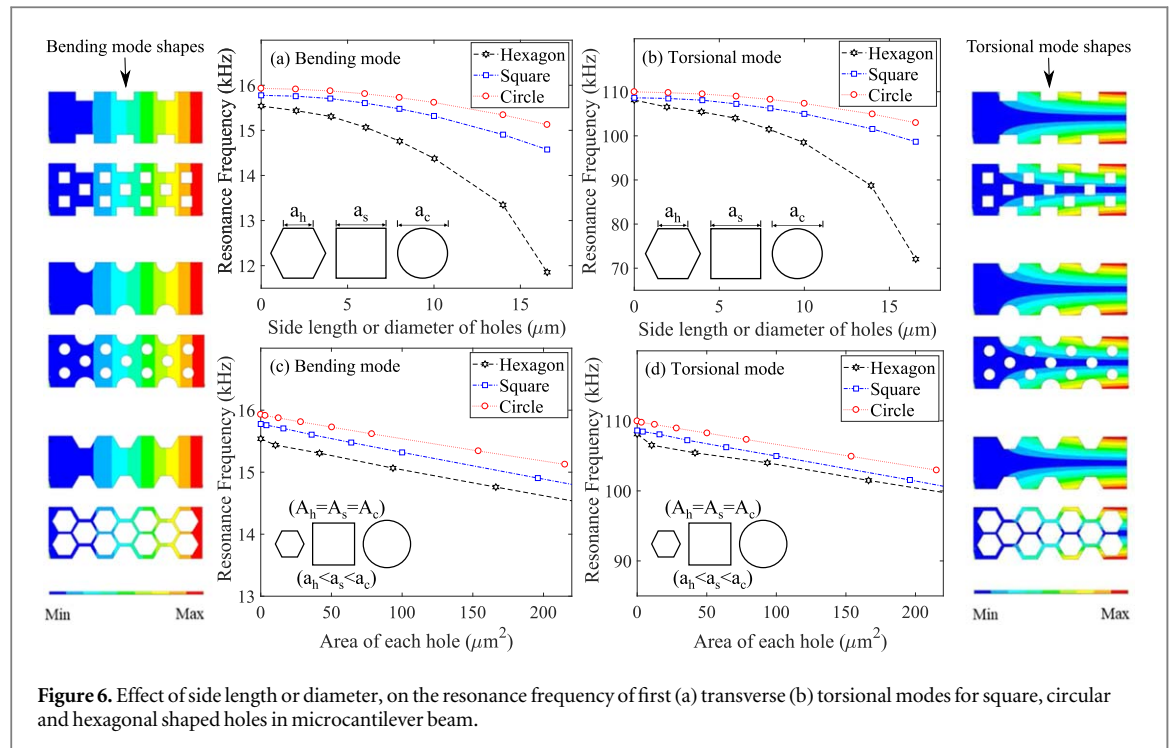
Hexagon side length 'a' (μm)	Resonance frequency (kHz)					
	Transverse mode			Torsional mode		
	Experimental	Numerical	Error (%)	Experimental	Numerical	Error (%)
Zero	16.15	15.53	3.8	114.39	108.11	5.48
16.55	11.30	11.85	4.6	72.49	72.05	0.6

holes ($a_h = a_s = a_c$) are kept constant, i.e. 16.55 μm , while in the second case, area of holes are kept constant such that side length of square hole is obtained as ($a_s = \sqrt{\frac{3\sqrt{3}}{2}} \cdot a_h$) and the diameter of circular hole is obtained as $a_c = \sqrt{\frac{6\sqrt{3}}{\pi}} \cdot a_h$, respectively, where a_h is the side length of the hexagonal holes. It is clearly seen that for the same side length or diameter, beam with the hexagonal shaped holes gives the highest static deflection, which is 208.78% and 248.87% higher than the beams with square and circular holes, respectively. It suggests that hexagonal hole indeed enhances flexibility. For completeness, in second case in which for same area of hexagonal hole with side length $a_h = 16.55 \mu\text{m}$, a_s and a_c are found as 26.68 μm and 30.10 μm which are larger than that of hexagonal hole. Consequently, the static deflection of beam with square hole is nearly same and beam with circular hole is relatively low as compared to beam with hexagonal hole of same area. Thus, we found that the presence of holes makes the beam more flexible, and beam with hexagonal hole shape provides the maximum deflection for the same side lengths or diameter of other hole shaped beams.

To understand the influence of hexagonal holes on frequencies, we measured first bending mode frequencies of hexagonal beams without and with holes as 16.15 kHz and 11.30 kHz, respectively, as mentioned in table 2. The frequency of beam with holes is reduced by 30% as compared to that without any holes. The corresponding first torsional mode frequency of beam with holes measured as 72.49 kHz which is about 36% lower than that of the beam without any holes.

To discuss the influence of hexagonal holes with side length $a = 0$ and $a = 16.55 \mu\text{m}$ in microcantilever beam with honeycomb shape, we also perform modal analysis to compute first bending mode and first torsional mode based on FEM simulation as mention in table 2. The numerical values are found to be in agreement with measured values with maximum percentage error of about 5% as mentioned in table 2.

To systematically study the influence of holes and their different geometrical shapes on first bending and first torsional frequencies, we numerically compute mode shapes and frequencies of beams with varying the hole size ($(a_h, a_s$ and $a_c)$) from 0 to 16.55 μm as shown in figures 6(a) and (b), respectively. The corresponding bending and torsional mode shapes of microcantilever beams having various hole shapes are also shown on the left side of figure 6(a) and right side of figure 6(b), respectively. Based on the variation of frequencies of with hole side length or diameter, 'a', we found that the frequencies of both transverse and torsional modes decrease with the increase in hole size which is mainly due to reduction in stiffness of the beam. We can also see that the maximum variation is found in honeycomb shaped microcantilever beam. Thus, it can be summarized that the presence of hexagonal, square and circular holes with side length $a = 16.55 \mu\text{m}$ of microcantilever beams reduces the frequency by 28.62%, 12.24% and 8.92%, respectively, and the static deflection increases by 454.18%, 79.77% and 58.85%, respectively, as compared to the equivalent rectangular beam. Thus, honeycomb shaped beam with



hexagonal hole shape increases the flexibility but reduces the bending and torsional frequencies. To explore the means to increase its frequency with given hole size, we cover the beam with nanofiber mat and study its effect in tuning the frequency of beam and nanofiber composite in the next section.

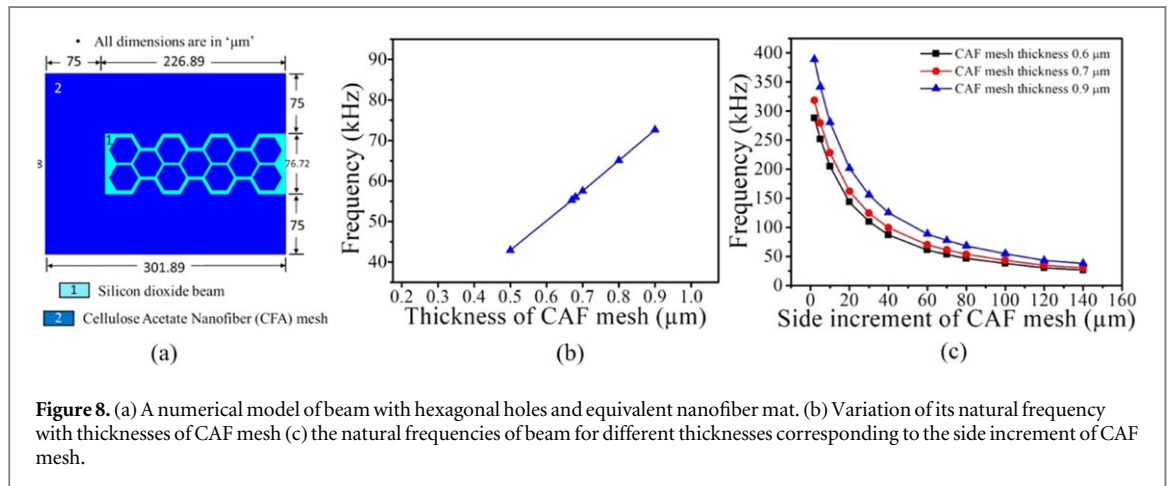
3.3. Frequency analysis of microbeams with nanofibers mat

In this section, we present experimental and numerical analysis of honeycomb shaped microcantilever beams without and with cellulose acetate nanofibers (CAFs) mat. The measurement procedure and numerical procedure in modeling the structures and nanofiber mats have been presented in sections 2.1 and 2.2, respectively. In this section, first, we describe procedure to extract nanofibers mat parameters with appropriate boundary conditions. After we validate the numerical model with experimental results with selected material properties and boundary condition, we apply it to compute the frequency of honeycomb-shaped hexagonal beam without and with CAFs mat.

To extract the nanofibers mat parameters and appropriate boundary condition, we take a die contain suspended microbeams with thickness $0.962 \mu\text{m}$ covered uniformly with nanofiber mat. Considering honeycomb-shaped microcantilever having length and width as $226.89 \mu\text{m}$ and $76.72 \mu\text{m}$ with hexagonal hole of side length $a = 16.55 \mu\text{m}$. Figures 7(b) and (d) show measured frequency response curves with mode shapes for honeycomb-shaped beam with hexagonal holes without and with nanofiber mat. The measured frequencies of first transverse bending mode of beam without and with nanofibers mat are compared in table 3. It shows that the frequency of beam is significantly improved by 359%. Thus, it is shown that interfacing nanofibers mat can improve the frequency of hexagon beam with holes even beyond the frequency of hexagon beam without holes. However, presence of nanofibers mat is found to adversely affect the quality factors in all the design. The mechanism of damping due to interaction of nanofiber mats and microbeam can be further studied in future.

Table 3. Comparison of resonance frequency and Q-factor corresponding to first transverse mode for different designs of SiO₂ microcantilever beam for without and with CAFs mesh.

Cantilever type	Without fibers		With fibers	
	Frequency (kHz)	Q-factor	Frequency (kHz)	Q-factor
Present model	12.09	806.26	55.51	37.76

**Figure 8.** (a) A numerical model of beam with hexagonal holes and equivalent nanofiber mat. (b) Variation of its natural frequency with thicknesses of CAF mesh (c) the natural frequencies of beam for different thicknesses corresponding to the side increment of CAF mesh.**Table 4.** Comparison of numerical and experimental resonance frequencies for the design of hexagonal-shaped SiO₂ microcantilever beam corresponding to without and with CAF mat.

Beam details	SiO ₂ beam thickness (μm)	CAF mat thickness (μm)	Side increment (μm)	Frequency (kHz)	
				Without CAF mat (Num./Exp.)	With CAF mat (Num./Exp.)
Present model	0.962	0.67	75	12.005/12.09	55.268/55.51

To numerically model the beams, we build numerical models of given design with required dimensions in ANSYS as shown in figure 8(a). The elastic modulus, density and Poisson's ratio are taken as 120 MPa, 1.28 g cm⁻³ and 0.3, respectively, which are in the range of CAFs mats found in the literature [28, 29]. Considering simply-supported boundary condition, we model nanofiber on microcantilever beam as shown in figure 8(a). Subsequently, we vary the thickness of nanofibers mat for the given hexagonal microcantilever beam, then compute the frequency variations as shown in figure 8(b). The frequency increases linearly with nanofibers mat thickness. Investigating the influence of gap between side boundaries and hexagonal beam on its frequency, we found that as the distance increases the frequency decreases exponentially and become independent at larger side boundaries as shown in figure 8(c). These variations are also computed for three different values of nanofiber mat thickness. It is found that as nanofibers mat thickness increases, frequency increases. Thus, we found that the frequency is strong function of nanofiber mat thickness and gap between side boundaries and beam. Thus, for a given side boundaries, we find the thickness of equivalent nanofiber mat thickness based on the comparison between computed and experimental results as mentioned in table 4. The thickness of nanofiber mat is found as 0.67 μm.

After validating FEM model with identified physical properties of nanofiber mat based on experimental results, we discuss the influence nanofiber mat on hexagonal shaped beam with holes and equivalent rectangular beam in figure 9. We show that numerically computed frequency of solid rectangular beam without any holes is 16.6 kHz which can be increased to 22.64 kHz by simply coating its top surface with nanofiber mat. These numerical results are compared well with corresponding analytical results. Similarly, numerically computed frequency of beam with hexagonal shape having holes without nanofiber is 12 kHz and with nanofiber mat is 18 kHz. Such increment is due to simply coating the surface without any pretension. The analytical results based on elastic modulus found using the rule of mixture [27, 30] are found to be closure to the numerical results. Further, frequency tuning can be observed by providing pretension to the fibres from the side ways. In the present work, we have extended the surface of nanofiber mat beyond cantilever surface and taken it till the

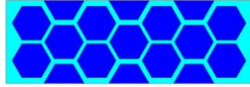

Type of beam	(a) Hexagonal shaped beam with CAF mat	(b) Equivalent rectangular beam with CAF mat
Simple schematic diagram of FE beam model		
Dimension	SiO ₂ beam	$L = 226.89\mu\text{m}, w = 76.72\mu\text{m}, t_{\text{SiO}_2} = 0.962\mu\text{m}$
	CAF mat	$L = 226.89\mu\text{m}, w = 76.72\mu\text{m}, t_{\text{CAF}} = 0.67\mu\text{m}$
Frequency (kHz)	without CAF mat	12.005
	with CAF mat	16.603 (FEM) 16.567 (Analytical)
	with CAF mat	18.091
		22.641 (FEM) 23.716 (Analytical)

Figure 9. Comparison of resonance frequencies of, (a) honeycomb-shaped microcantilever SiO₂ beam having hexagonal hole of side length $a = 16.55 \mu\text{m}$ with CAF mat of same length and width as $226.89 \mu\text{m}$ and $76.72 \mu\text{m}$ and (b) equivalent rectangular beam with CAF mat of similar dimensions as used to model the type (a) microcantilever beam model.

boundaries of cavity which provide simply-supported boundary condition. On analysing the influence of side cavity width and nanofiber thickness on frequency of hexagonal beam with coated nanofiber mat, we found that the frequency can be enhanced further by a large margin.

4. Conclusions

In this paper, to capture some of the properties of graphene which consists of repetitive patterns of hexagonal unit cell into 2D nanosheet, we have analyzed the influence of hexagonal shape of microcantilever beam with and without hexagonal hole of varying side length. To carry out the analysis, we fabricated the structure and performed measurement using laser vibrometer. Based on the measurement, we found that frequency of microcantilever beam with hexagonal shape decreases with increase in hole size. It is possibly due to decrease in stiffness or increase in beam flexibility. However, to confirm it, we numerically performed static analysis and found that the static deflection of hexagon-shaped beam with holes of length $a = 16.55 \mu\text{m}$, indeed, increases by 685% as compared to that of equivalent rectangular beam. Thus, microbeam having hexagonal shape with holes can inherit the flexibility property of 2D graphene material to some extent. However, it also has an adverse effect on frequency which decreases with hole size. In order to overcome this effect, we propose to put nanofibers mat on the top surface of microbeam to make a hierarchical structure. It is found that frequency can be tuned by changing the distance between beam and side boundaries, and the thickness of nanofibers mat. For the given dimensions of hexagon shape beam with holes, the frequency tuning of about 358% can be achieved when the side boundaries are located at a distance of $75 \mu\text{m}$ from the free sides of the beam.

Acknowledgments

The research is supported in part by the Council of Scientific and Industrial Research (CSIR), India (22(0696)/15/EMR-II). The author AG acknowledges the fellowship provided by the Department of Higher Education, Ministry of Human Resource Development, Government of India, and RCI Hyderabad.

ORCID iDs

Akarapu Ashok  <https://orcid.org/0000-0003-1442-5088>

Chandra Sekhar Sharma  <https://orcid.org/0000-0003-3821-1471>

Ashok Kumar Pandey  <https://orcid.org/0000-0002-5878-6451>

References

- [1] Ko F, Gogotsi Y, Ali A, Naguib N, Ye H, Yang G, Li C and Willis P 2003 *Adv. Mater.* **15** 1161–5
- [2] Gangele A, Sharma C S and Pandey A K 2017 *J. Nanosci. Nanotechnol.* **17** 2256–73

- [3] Tang L, Yang Z, Duan F and Chen M 2017 *Colloids Surf., A* **520** 184–92
- [4] Gay T, Kaufman J and McGuigan M 2005 *Power Point Slides given at Boston University* Available at http://www.bu.edu/gk12/marc/Lessons/cnt/cnt_talk.pdf
- [5] Kumar L, Jenni L V, Haluska M, Roman C and Hierold C 2018 *AIP Adv.* **8** 025118
- [6] Daraio C, Nesterenko V F, Jin S, Wang W and Rao A M 2006 *J. Appl. Phys.* **100** 064309
- [7] Teo E H, Yung W K, Chua D H and Tay B 2007 *Adv. Mater.* **19** 2941–5
- [8] Mesarovic S D, McCarter C M, Bahr D F, Radhakrishnan H, Richards R F, Richards C D, McClain D and Jiao J 2007 *Scr. Mater.* **56** 157–60
- [9] Pathak S, Cambaz Z G, Kalidindi S R, Swadener J G and Gogotsi Y 2009 *Carbon* **47** 1969–76
- [10] Agnihotri N, Chowdhury A D and De A 2015 *Biosens. Bioelectron.* **63** 212–7
- [11] Tian M, Qu L, Zhang X, Zhang K, Zhu S, Guo X, Han G, Tang X and Sun Y 2014 *Carbohydrate Polym.* **111** 456–62
- [12] Blakri R, Sayari A, Shalaan E, Wageh S, Al-Ghamdi A A and Bouazizi A 2014 *Superlattices Microstruct.* **76** 461–71
- [13] Yang J, Ono T and Esashi M 2000 *Sens. Actuators, A* **82** 102–7
- [14] Amorim B et al 2016 *Phys. Rep.* **617** 1–54
- [15] Kang J, Hwang S, Kim J H, Kim M H, Ryu J, Seo S J, Hong B H, Kim M K and Choi J B 2012 *ACS Nano* **6** 5360–5
- [16] Zande A M V D, Barton R A, Alden J S, Ruiz-Vargas C S, Whitney W S, Pham P H Q, Park J, Parpia J M, Craighead H G and McEuen P L 2010 *Nano Lett.* **10** 4869–73
- [17] Goossens S et al 2017 *Nat. Photonics* **11** 366 EP-article
- [18] Wang Q, Hong W and Dong L 2016 *Nanoscale* **8** 7663–71
- [19] Todorović D, Matković A, Miličević M, Jovanović D, Gajić A, Salom I and Spasenović M 2015 *2D Materials* **2** 045013
- [20] Thomas B, Raj M C, Joy J, Moores A, Drisko G L and Sanchez C 2018 *Chem. Rev.* **18** 11575–625
- [21] Ashok A, Kumar P M, Singh S S, Raju P, Pal P and Pandey A K 2018 *Sens. Actuators, A* **273** 12–8
- [22] Kumar P and Vasita R 2017 *J. Appl. Polym. Sci.* **134** 45012–1–11
- [23] Mohamed A, Osman T, Toprak M S, Muhammed M and Uheida A 2017 *Chemosphere* **180** 108–16
- [24] Nasir M, Matsumoto H, Danno T, Minagawa M, Irisawa T, Shioya M and Tanioka A 2006 *J. Polym. Sci., Part B: Polym. Phys.* **44** 779–86
- [25] Kakunuri M, Wanasekara N D, Sharma C S, Khandelwal M and Eichhorn S J 2017 *J. Appl. Polym. Sci.* **134** 44709-1-7
- [26] 2013 ANSYS Mechanical APDL 15.0-Basic Analysis Guide <https://www.ansys.com/en-in/products/structures/ansys-mechanical-enterprise>
- [27] Ashok A, Gangele A, Pal P and Pandey A K 2018 *J. Micromech. Microeng.* **28** 075009
- [28] Stylianopoulos T, Kokonou M, Michael S, Tryfonos A, Rebholz C, Odysseos A D and Doumanidis C 2012 *Journal of Biomedical Materials Research Part B: Applied Biomaterials* **100** 2222–30
- [29] Salama A, Mohamed A, Aboamera N M, Osman T and Khattab A 2018 *Adv. Polym. Tech.* **37** 2446–51
- [30] Gangele A and Pandey A K 2018 *Int. J. Mech. Sci.* **142-143** 491–501